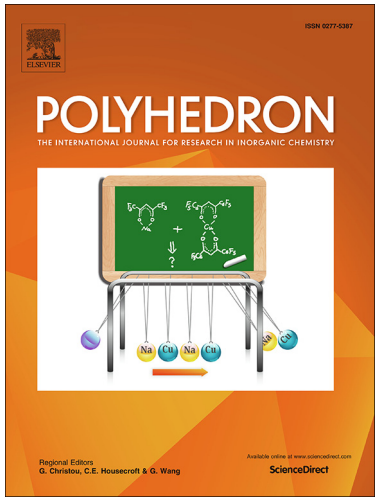

Synthesis, structure and diverse coordination chemistry of cobalt(III) complexes derived from a Schiff base ligand and their biomimetic catalytic oxidation of *o*-aminophenols

Narayan Ch. Jana, Moumita Patra, Paula Brandão, Anangamohan Panja

PII: S0277-5387(19)30125-1
DOI: https://doi.org/10.1016/j.poly.2019.02.024
Reference: POLY 13768

To appear in: *Polyhedron*

Received Date: 11 November 2018
Revised Date: 10 February 2019
Accepted Date: 13 February 2019

Please cite this article as: N.C. Jana, M. Patra, P. Brandão, A. Panja, Synthesis, structure and diverse coordination chemistry of cobalt(III) complexes derived from a Schiff base ligand and their biomimetic catalytic oxidation of *o*-aminophenols, *Polyhedron* (2019), doi: https://doi.org/10.1016/j.poly.2019.02.024

Synthesis, structure and diverse coordination chemistry of cobalt(III) complexes derived from a Schiff base ligand and their biomimetic catalytic oxidation of *o*-aminophenols

Narayan Ch. Jana,[a‡] Moumita Patra,[a‡] Paula Brandão,[b] and Anangamohan Panja[*a]

[a] *Postgraduate Department of Chemistry, Panskura Banamali College, Panskura RS, WB 721152, India*

[b] Department of Chemistry, CICECO-Aveiro Institute of Materials, University of Aveiro, 3810-193 Aveiro, Portugal

[*]Corresponding Author

E-mail: ampanja@yahoo.co.in

‡ These authors contributed equally to this work.

This paper deals with the syntheses and structural characterizations of four new cobalt(III) compounds (**1–4**) derived from a N_3O donor Schiff base ligand and their catalytic activity towards the aerobic oxidation of *o*-aminophenols. Both counter ions and solvents used for the synthesis have significant influence on structural diversity of the resulting complexes. X-ray crystallography reveals that although the geometry of cobalt(III) centres are octahedral in all the cases but the coordination environments are significantly different in them. All these complexes show diverse reactivity towards the catalytic oxidation of *o*-aminophenols in which availability of substitutaionally labile sites at the metal centre for substrate *o*-aminophenols binding is the main reason for higher catalytic activity in **2** and **3** than others. Furthermore, we have examined the detailed kinetic studies of the aerobic oxidation of one substituted *o*-aminophenol, namely 2-amino-5-methylphenol, using **2** and **3** as catalysts in

which facile oxidation of the substituted *o*-aminophenol was noticed. ESI mass spectral study has been carried in order to get insight into mechanistic pathway of functioning such catalytic activity.

Keywords: Cobalt complexes, Structural diversity, Influence of coordination sphere on catalytic activity, Phenoxazine chromophores, Mass spectrometry and proposed mechanism

1. Introduction

Most of the industrial oxidation processes for the synthesis of various organic chemicals including the manufacture of large-scale pharmaceutical compounds use permanganate, dichromate and heavy metal oxides as oxidants, leading to the environmental pollution [1,2]. However, in the natural oxidation process, dioxygen is used as sole oxidant for the biocatalytic oxidation of various biologically important organic compounds where the metalloenzymes activate dioxygen [3−11]. Therefore, the biomimetic studies of these metalloenzymes could provide us valuable catalysts for *in vitro* synthesis of various organic compounds using dioxygen as a primary oxidant [12−16]. Further studies with these biomimetic models may help for better understanding of the mechanistic aspects occurring at the active site of the metalloenzymes [17−23]. Though a decent effort has been made by the bioinorganic chemists in unravelling the catalytic mechanism of action of these enzymes by means of a synthetic analogue approach, [24−26] further mechanistic studies are required for developing alternative pathways to form same products.

We have been developing biomimetic catalysts for the oxidation of 3,5-di-*tert*-butylcatechol [27−29] and *o*-aminophenol [30,31] by molecular dioxygen mimicking the function of catechol oxidase and phenoxazinone synthase, respectively. Transition metal complex mediated oxidative coupling of *o*-aminophenol to 2-aminophenoxazinone through catalytic activation of dioxygen has been considered as an important reaction [32−34]

because of the presence of 2-aminophenoxazinone chromophore in actinomycin D, a naturally occurring antibiotic [35]. Actinomycin D is among the most potent antineoplastic agents known to inhibit DNA directed RNA synthesis [36,37]. It is used for the treatment of some kind of cancers of the bones and soft tissues like choriocarcinoma, testis, Wilms' tumor, rhabdomyosarcoma, Kaposi's sarcoma and Ewing's sarcoma [38]. Although biological activity of actinomycin was elucidated, other phenoxazine derivatives have not been examined well. Recently, Tomoda and co-workers were examined the anti-bacterial effects of Phx-1 (2-aminophenoxazinone), Phx-2 (2-amino-4,4a-dihydro-4a-7-dimethyl-3*H*-phenoxazinone) and Phx-3 (3-amino-1,4a-dihydro-4a-8-dimethyl-2*H*-phenoxazinone) (Scheme 1), which are produced by the reaction of *o*-aminophenol or its derivatives with bovine hemoglobin [39]. Thus, the chemistry of phenoxazine derivatives has to be further explored. The active site structures of the metalloenzymes and their efficient synthetic models [28−35,40−48] disclose that the redox flexibility of the metal centers and the labile position(s) at metal sites are crucial factors behind their efficient activities. Therefore, the ligands with fewer donor sites are more suitable for the development of efficient synthetic analogues.

The coordination chemistry of *N*,*N*-dimethyldipropylenetriamine is almost unexplored, [49] and we recently reported a series of Ni(II) and Co(III) complexes [50] with Schiff base ligands resulting from this triamine with substitutionally labile coordination sites in most cases. In continuation of our research interest, [27−31] we report, herein, the synthesis and structures of four new cobalt complexes, $[Co(HL)_2](ClO_4)_3 \cdot 2H_2O$ **(1)**, $[Co(L)(N_3)_2]$ (**2**), $[Co(L)(NCS)_2]$ (**3**), and $[Co(L)(Br\text{-}sal)]_2[Co(NCS)_4]$ **(4)** (where HL is a Schiff base ligand as shown in scheme 2 and Br-salH is 5-bromosalicylaldehyde), and their biomimetic catalytic activity using the substrates *o*-aminophenol and 2-amino-5-methylphenol by molecular dioxygen. Remarkable influence of solvents and counter ions leading to the diverse

coordination chemistry of cobalt was observed. Further emphasis was given to ESI mass spectral study to get insight into the mechanism of action of such catalytic activity.

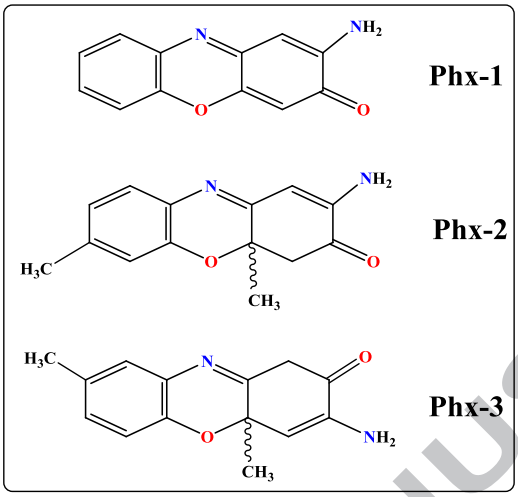

Scheme 1: Chemical structures of Phx-1, Phx-2, and Phx-3.

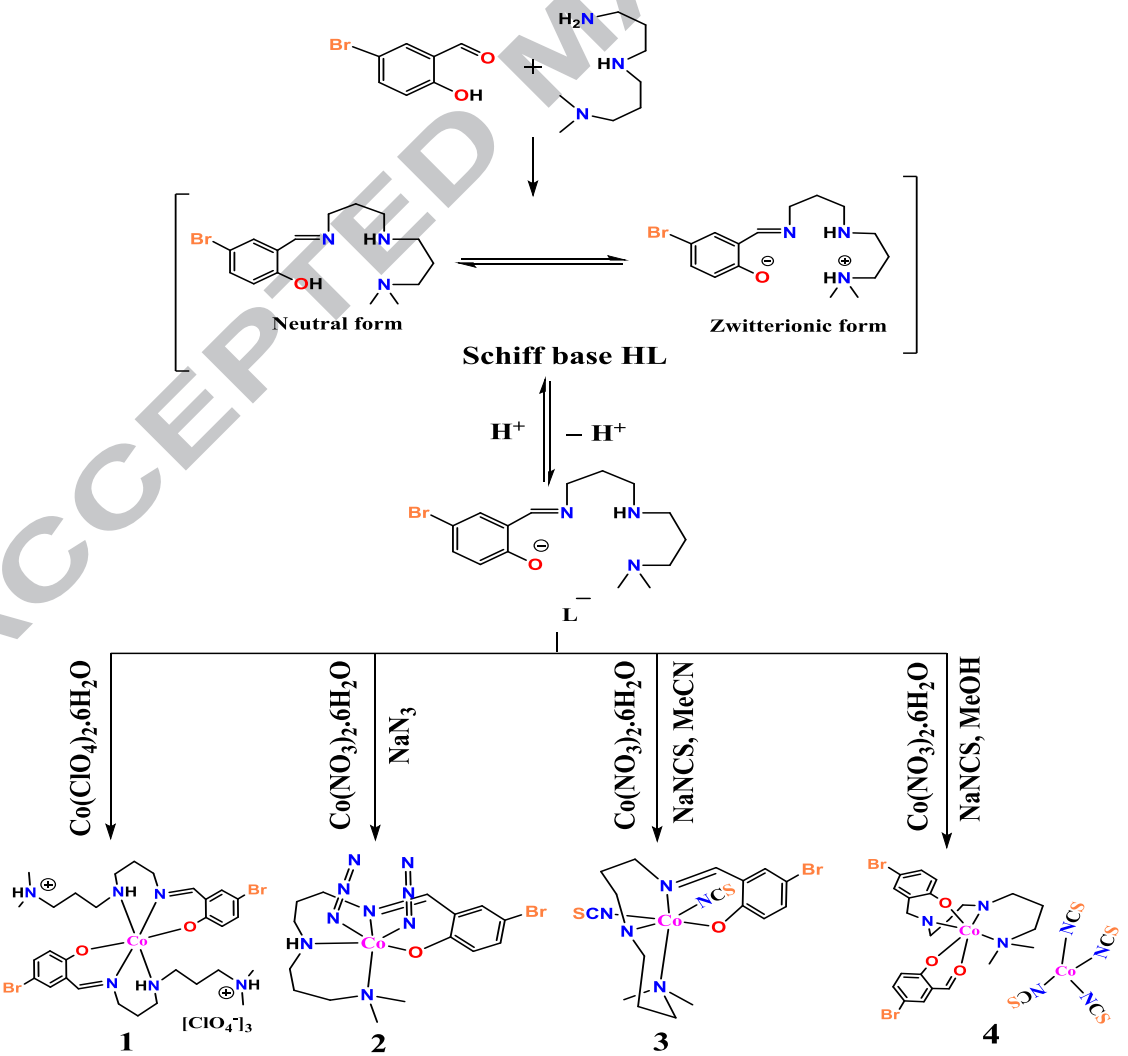

Scheme 2. Schiff base HL and synthetic scheme.

2. Experimental section

2.1 Materials and physical measurements

Cobalt(II) nitrate hexahydrate, cobalt(II) perchlorate hexahydrate, *o*-aminophenol (OAPH), 5-bromosalicylaldehyde (Br-salH), and *N*,*N*-dimethyldipropylenetriamine were of commercially available reagent or analytical grade chemicals and were used as received. 2-amino-5-methylphenol was purchased from Alfa Aesar. Other chemicals and solvents were of reagent grade and used without further purification.

Caution! Metal perchlorate and azide salts are potentially explosive. Although no problem was encountered in the present study, use of small amounts of the materials with great precaution is recommended.

CHN (carbon, hydrogen and nitrogen) analysis were performed using a Perkin-Elmer 240C elemental analyser. Electronic absorption spectra were recorded using an Agilent Carry-60 diode array UV-Vis spectrophotometer at room temperature with a 1-cm path-length quartz cell. IR spectra were performed in a PerkinElmer Spectrum Two FTIR spectrophotometer in the range 400 to 4000 cm^{-1} with the samples prepared as KBr pellets. Electrochemical studies were performed using tetrabutylammonium perchlorate as a supporting electrolyte in methanol on a CH Instrument electrochemical workstation model CHI630E, with the conventional three-electrode assembly comprising of a platinum working electrode, a platinum wire auxiliary electrode and a Ag/AgCl reference electrode. Electrospray ionization mass spectral (ESI-MS positive) study were conducted in a Micromass Q-tof-Micro Quadruple mass spectrometer. ^{1}H NMR spectra were measured using a Bruker 300 spectrometer in DMSO-d_6. Magnetic susceptibility measurement was carried out on a PAR 155 vibrating sample magnetometer at room temperature.

2.2 Synthesis of the Schiff-base ligand (HL)

A mixture of 1.0 mmol of *N,N*-dimethyldipropylenetriamine (159 mg) and 1.0 mmol of 5-bromosalicylaldehyde (166 mg) in 20 ml of methanol was heated to reflux for about 1 h, turning down a dark yellow solution. The solvent was removed under reduced pressure that resulted dark yellow crude oily ligand. The same was extracted with dichloromethane and the solvent was removed under reduced pressure that resulted finally the dark yellow liquid ligand with desired purity. Anal. Calcd. for $C_{30}H_{52}Br_2Cl_3CoN_6O_{16}$: C 52.64%, H 7.07%, N 12.28 %. Found: C 51.37%, H 7.28%, N 12.03 %. FTIR (KBr, cm^{-1}): *ν*(C=N) 1635 s; *ν*(N–H/O–H) 3326 br.

2.3 Synthesis of $[Co(HL)_2](ClO_4)_3 \cdot 2H_2O$ (**1**)

A methanol solution of cobalt(II) perchlorate hexahydrate (366 mg, 1.0 mmol) was added to a methanol (20 ml) solution of the Schiff base ligand HL (2.0 mmol) with stirring. Instantly the solution became dark-brown colour and it was further stirred in air for 1 h. The reaction mixture was filtered and left undisturbed for slow evaporation of solvent. Dark-brown colour crystals suitable for X-ray diffraction were separated out from the solution at ambient temperature within few days, which were collected by filtration and washed with methanol/ether and air dried. Yield: 866 mg (81 %). Anal. Calcd. for $C_{30}H_{52}Br_2Cl_3CoN_6O_{16}$: C 33.52%, H 4.88%, N 7.82 %. Found: C 33.67%, H 4.78%, N 7.63 %. FTIR (KBr, cm^{-1}): *ν*(C=N) 1624 s; *ν*(ClO_4) 624 s, 1080 s.

2.4 Synthesis of $[Co(L)(N_3)_2]$ (**2**)

Cobalt(II) nitrate hexahydrate (291 mg, 1.0 mmol) in 20 ml of methanol was added to the Schiff base ligand HL (1.0 mmol) solution with stirring, which instantaneously produced a dark-brown solution. The mixture was further stirred in air for 30 min, and to this solution

sodium azide (130 mg, 2.0 mmol) in methanol/water (5 ml, 4:1 v/v) was slowly added with stirring. The resulting solution was allowed to reflux for about 30 min and it was then filtered and kept at ambient temperature for slow evaporation, which afforded X-ray diffraction quality dark-brown crystals after few days. These crystals were collected by filtration and washed with methanol/ether and air dried. Yield: 373 mg (77 %). Anal. Calcd. for $C_{15}H_{23}BrCoN_9O$: C 37.21%, H 4.79%, N 26.03 %. Found: C 37.29%, H 4.60%, N 25.91 %. FTIR (KBr, cm^{-1}): $\nu(N_3)$ 2032 vs; ν(C=N) 1618 s.

2.5 Synthesis of complex $[Co(L)(NCS)_2]$ (**3**)

Complex **3** was synthesized from acetonitrile/water (20:1, v/v) mixture adopting the identical procedure as described for **2,** except that NaSCN was used instead of NaN_3. Colour: Dark brown, Yield: 387 mg (75%). Anal. Calcd. for $C_{17}H_{23}BrCoN_5OS_2$: C 39.54 %, H 4.49%, N 13.56 %. Found: C 39.63%, H 4.40%, N 13.49 %. FTIR (cm^{-1}, KBr): ν(NCS) 2065 s, ν(C=N) 1625 s.

2.6 Synthesis of complex $[Co(L)(Br\text{-}sal)]_2[Co(NCS)_4]$ (**4**)

Complex **4** was synthesized from methanol/water (20:1, v/v) mixture following same procedure as that applied for the synthesis of **2**, but NaSCN was used in place of NaN_3. Colour: Dark brown, Yield: 343 mg (69%). Anal. Calcd. for $C_{48}H_{54}Br_4Co_3N_{10}O_6S_4$: C 38.65%, H 3.65%, N 9.39 %. Found: C 38.69%, H 3.57%, N 9.30%. FTIR (cm^{-1}, KBr): ν(NCS) 2063 s, ν(C=N) 1623 s.

2.7 X-ray crystallography

Suitable single crystals for all complexes were chosen for X-ray diffraction, and the data were collected on a Bruker SMART APEX-II CCD X-ray diffractometer, which is equipped with a graphite-monochromated Mo Kα (λ = 0.710 73 Å) radiation by the ω-scan method. Data integration, reduction, and space group determination were performed using using the SAINT-plus software, and the absorption correction was made by multi-scan method using

SADABS program [51]. The structures were solved using the direct method and refined by the successive full-matrix least-squares cycles on F^2 using SHELXL-v.2013 or SHELXL-v.2014 [52]. Anisotropic refinement was performed for all non-hydrogen atoms while the hydrogen atoms placed on carbon atoms were refined using fixed geometry and riding thermal parameters. The hydrogen atoms associated with nitrogen atoms were located on the difference Fourier map and isotropically treated with fixed thermal parameters equivalent to 1.2 times of the parent atoms. All the crystallographic diagrams for **1**–**4** were generated with the MERCURY-3.10.1 software. Information regarding the X-ray diffraction data collection and structure refinements of the compounds is given in Table 1.

Table 1. Crystallographic data and structure refinement parameters of **1** to **4**

	1	**2**	**3**	**4**
Empirical formula	$C_{30}H_{46}Br_2Cl_3CoN_6O_{16}$	$C_{15}H_{23}BrCoN_9O$	$C_{17}H_{23}BrCoN_5OS_2$	$C_{48}H_{54}Br_4Co_3N_{10}O_6S_4$
Formula weight (g mol^{-1})	1071.83	484.26	516.36	1487.70
Crystal system	Monoclinic	Monoclinic	Monoclinic	Monoclinic
Space group	*C2/c*	*P2$_1$/c*	*P2$_1$/c*	*C2/c*
a (Å)	20.3477(18)	11.5230(2)	10.2789(6)	11.4638(3)
b (Å)	13.8596(13)	9.2719(2)	13.1774(7)	23.0995(7)
c (Å)	16.2643(14)	18.9789(4)	15.6068(9)	21.5616(7)
α(°)	90	90	90	90
β(°)	107.420(3)	106.2820(10)	93.700(3)	99.484(2)
γ(°)	90	90	90	90
volume (Å^3)	4376.3(7)	1946.38(7)	2109.5(2)	5625.6(3)
Z	4	4	4	4
D_{calc} (mg m^{-3})	1.625	1.653	1.626	1.757
μ (mm^{-1})	2.473	2.961	2.923	3.198
F(000)	1908	984	1048	2972
θ Range (°)	2.625–27.219	1.841–27.922	1.985–26.443	1.763–27.152
Reflections collected	40409	17294	14714	43974
Independent reflections (R_{int})	4788(0.0621)	4654(0.0412)	4328(0.0628)	6243(0.0505)
Observed reflections [I>2σ(I)]	4357	3727	2865	5101
Restraints/parameters	2/246	0/250	0/250	0/355
Goodness-of-fit on F^2	1.119	1.028	1.006	1.129
Final *R* indices [I>2σ(I)]	R_1 = 0.1401 wR_2 = 0.2934	R_1 = 0.0392 wR_2 = 0.0892	R_1 = 0.0408 wR_2 = 0.0784	R_1 = 0.0464 wR_2 = 0.0920
R indices (all data)	R_1 = 0.1482 wR_2 = 0.2978	R_1 = 0.0551 wR_2 = 0.0964	R_1 = 0.0822 wR_2 = 0.0910	R_1 = 0.0607 wR_2 = 0.0965
Largest diff. peak/hole (e Å^{-3})	2.074/ –1.856	1.457/ –0.660	0.596/ –0.649	1.293/ –0.849

2.8 Catalytic oxidation of o-aminophenols

The phenoxazinone synthase like activity was carried out by the reaction of 1.0×10^{-2} M of *o*-aminophenol with 5×10^{-5} M of the complexes (**1**–**4**) in air saturated methanol at room temperature. Similarly, the oxidation reaction of 2-amino-5-methylphenol ($0.5–1.0 \times 10^{-2}$ M) was studied with **2** or **3** ($1.0–5.0 \times 10^{-5}$ M) in methanol. Kinetics of the aerobic oxidation of OAPH catalysed by **1**–**4** was investigated monitoring increase of the absorbance as a function of time at 435 nm, which is characteristic absorption band of 2-aminophenoxazinone in methanol. Similarly, the absorbance versus wavelength plots were generated for the reaction mixtures of substituted aminophenol and **2** (or **3)** by recording spectrophotometric data at a regular time interval of 5 min. The rate dependency on the substrate concentration was checked by the reaction of 1×10^{-5} M solution of the complexes with varying concentration of the substrate maintaining the pseudo-first-order condition All the kinetic measurements were carried out for a period of 10 min and the initial rate of the reaction was evaluated by the linear regression from slope of the absorbance verses time plot. Finally, various kinetic parameters were evaluated applying Michaelis–Menten model.

3. Results and Discussion

3.1 Syntheses and general characterizations

The ligand HL employed in the present study was synthesized by the Schiff base condensation reaction between 5-bromosalicylaldehyde and *N*,*N*-dimethyldipropylenetriamine in a 1: 1 molar ratio in refluxing methanol (Scheme 2). The Schiff base was isolated as an oily mass and that has been characterized by elemental

analysis, IR spectroscopy (*vide supra*) and NMR spectroscopy (see Fig. S1). This Schiff base ligand by the reaction with cobalt(II) perchlorate hexahydrate in a 2:1 molar ratio afforded $[Co(HL)_2](ClO_4)_3 \cdot 2H_2O$ (**1**) in high yield. Again this Schiff base ligand upon reaction with cobalt(II) nitrate hexahydrate together with pseudohalides (N_3^- for **2**, NCS^- for **3** and **4**) in a 1:1:2 molar ratio produced $[Co(L)(N_3)_2]$ (**2**), $[Co(L)(NCS)_2]$ (**3**) and $[Co(L)(Br\text{-}sal)]_2[Co(NCS)_4]$ (**4**), in high yields. All the above reactions are not dependent on stoichiometric ratios of the reactants, but significant influence of the solvents on product formation was observed. The reaction of the Schiff base ligand, cobalt nitrate hexahydrate and sodium thiocyanate in acetonitrile/water mixture resulted only isolable product **3**; but same reaction when carried out in methanol/water mixture only compound **4** was isolated in high yield. Following the same synthetic procedure, isolation of two different kinds of products clearly suggests that both of them are thermodynamic products where the relative stabilities in a particular solvent system governs the identity of the species that crystallizes from that solvent. Interestingly, compound **3** can be converted to complex **4** by prolong reaction in methanol/water mixture, which was further accelerated by the addition of Br-sal externally. As found in most of the Schiff base ligands with phenolic group, cobalt(II) centre is air-oxidized to cobalt(III) when it is bonded to the Schiff base. Some of the compounds have been characterized by NMR spectroscopy and the NMR data nicely agree with coordination of the Schiff base ligand to cobalt(III) metal centre (Figs. S2-S4).

The IR spectra of all complexes consist of sharp distinct bands due to stretching vibrations of the azomethine bond of the Schiff base appearing in the range 1615–1626 cm^{-1}. Additionally, the presence of a shoulder at around 1650 cm^{-1} is consistent with the C=O stretching frequency of the coordinated 5-bromosalicylaldehyde ion in **4**. Moreover, broad absorption bands at around 1080 and 624 cm^{-1} characteristics of the stretching and bending vibrations of perchlorate anion, respectively, are observed in the IR spectrum of complex **1**

[53]. The broadening of *ν*(Cl–O) band hints the participation of ClO_4^- ions in the hydrogen bonding interactions in the solid-state. In the IR spectrum of complex **2**, a strong absorption band is appeared at 2032 cm^{-1}, which is typical for stretching band of azide ion [54]. Bands at 2085 cm^{-1} and 2063 cm^{-1}, assignable to the stretching vibration of thiocyanate ions, are customarily noticed in the IR spectra of complex **3** and **4**, respectively [50a,57]. The better π acceptor ability of thiocyanate ion from cobalt(II) centre in **4** compared to its π acceptor ability from cobalt(III) in **3** is reflected from the relative stretching frequencies of thiocyanate ions in these complexes.

3.2 Structural descriptions

Single crystal X-ray diffraction studies were performed to determine the crystal structures of all complexes. The crystal structure of complex cation **1** together with selected atom numbering scheme is depicted in Fig. 1, while the molecular views of **2** and **3** are shown in Fig. 2, and Fig. 3 represents the crystal structure of **4**. The crystallographic parameters related to important bond distances around the metal coordination sphere for all structures are assembled in Table 2. Complex **1** crystalizes in the monoclinic C2/c space group where the complex cation of **1** sits on an inversion centre along with three non-coordinating disordered perchlorate anions, one of them residing on a two-fold rotation axis. The structure of the complex cation of **1** is a distorted octahedron in which two zwitterionic forms of the Schiff bases was coordinated to the metal centre. Each ligand coordinates the metal centre facially using one phenolate−O atom and two nitrogen atoms (one each of imine and secondary amine). The presence of zwitterionic form of Schiff base ligand is confirmed by the electro-neutrality of the system. The average Co−O and Co−N bond lengths are 1.889(6) and 1.986(7) Å, respectively, which are in good agreement with reported low spin octahedral cobalt(III) complexes [53,56,57].

Both **2** and **3** are neutral complexes and crystalize on general positions in the monoclinic $P2_1/n$ space groups. The crystal structure determination reveals that the geometry of the cobalt(III) centre is a distorted octahedral as reflected from slight deviation of *cisoid* (84.68(12)–93.66(11)°) and *transoid* (174.58(13)–177.14(13)°) angles from the ideal values. The structural features are similar in both cases where the phenolate-O and three nitrogen atoms (one each of imine, secondary amine and tertiary amine nitrogen atoms) of monoanionic Schiff base ligand together with two nitrogen atoms from two terminal azide (in **2**) and thiocyanate (in **3**) ions are bonded to the metal centre. Whereas three nitrogen atoms from triamine part of the Schiff base ligand occupy one meridional position, other meridional position is connected with two nitrogen atoms of pseudohalides and the phenolate-O atom of the Schiff base (Fig. S5). The Co–N(pseudohalide) and Co–O(phenolate) distances of the Schiff base ligand vary in the range 1.905(3)–1.961(3) and 1.874(2)–1.893(2) Å, respectively, and are comparable to reported low-spin octahedral cobalt(III) complexes [53,56,57]. The Co–N bond distances of imine, secondary and tertiary amines fall in the range 1.931(2)–1.933(3), 1.984(3)–2.001(3) and 2.084(3)–2.107(3) Å, respectively, in both complexes. The secondary amine bond is found somewhat longer than the imine nitrogen that is in agreement with their state of hybridisations. The presence of two methyl groups in tertiary nitrogen atom reduces Lewis basicity of the donor nitrogen atom, leading to the significantly longer bond distances of the tertiary amine in these complexes [50]. The solid-state stability of **2** is mainly governed by the hydrogen bonding interaction between secondary amine and one terminal nitrogen atom of coordinated azide ion from an adjacent molecule (Fig. 4). Further stability of the solid-state architecture of **2** is provided by the C–H···π interactions involving adjacent molecules. Similar kind of hydrogen bonding interaction is also observed in the solid-state structure of complex **3** in which the secondary amine forms hydrogen bond with the sulphur atom of coordinated thiocyanate ion from a neighbouring

molecule. Contribution from multiple C–H···π interaction involving two adjacent molecules is also noteworthy for overall stability of the solid-state structure of **3** (Fig 5).

Table 2. Important bond distances (Å) for complexes **1–4**.

Bond	**1**	**2**	**3**	**4**
Co(III)–N(imine)	1.949(8)	1.931(2)	1.933(3)	1.930(3)
Co(III)–N(secondary amine)	2.021(8)	2.001(3)	1.984(3)	2.005(3)
Co(III)–N(tertiary amine)	–	2.084(3)	2.107(3)	2.091(3)
Co(III)–O(phenolate)	1.887(7)	1.893(2)	1.874(2)	1.888(3)
Co(III)–O(free aldehyde)				1.884(3) 1.910(3)
Co(III)–N(pseudohalide)		1.961(3) 1.952(3)	1.916(3) 1.905(3)	
Co(II)–N(pseudohalide)		–	–	1.960(4) 1.947(4)

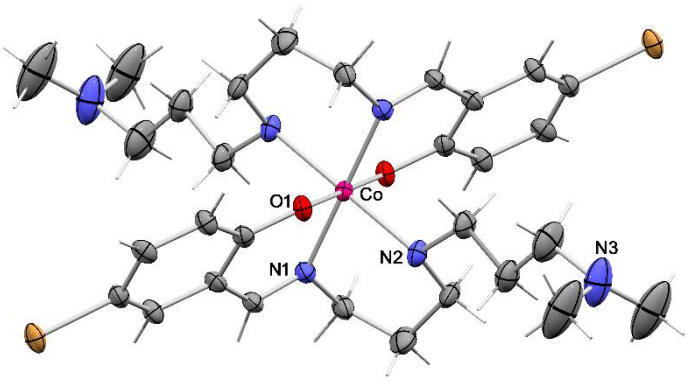

Fig. 1. Molecular structure of the complex cation of **1** with selected atom numbering scheme. The counter anions and water molecules were omitted for clarity the counter anions and water molecules were omitted for clarity. Thermal ellipsoids are drawn at 30% probability.

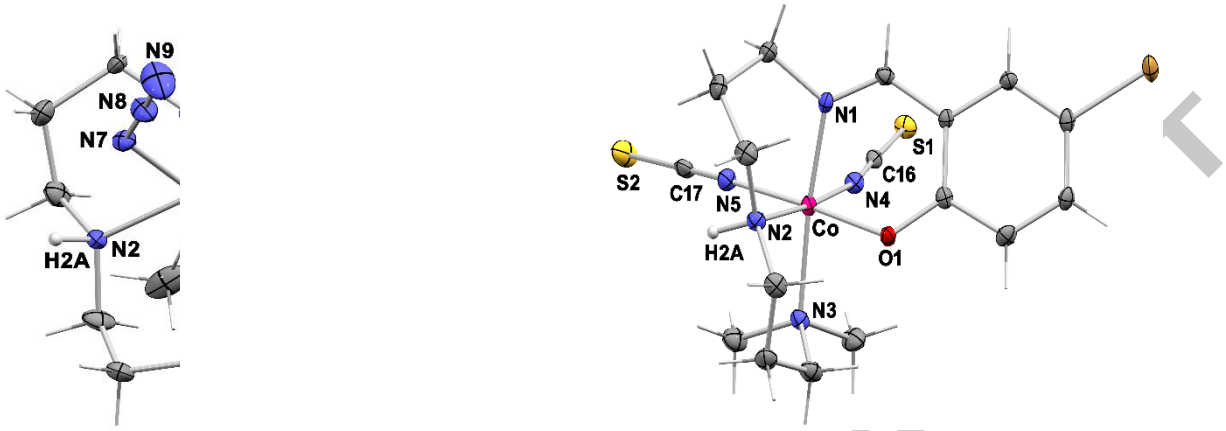

2 **3**

Fig. 2. Crystal structures of **2** and **3** showing selected atom numbering schemes. Thermal ellipsoids are drawn at 30% probability.

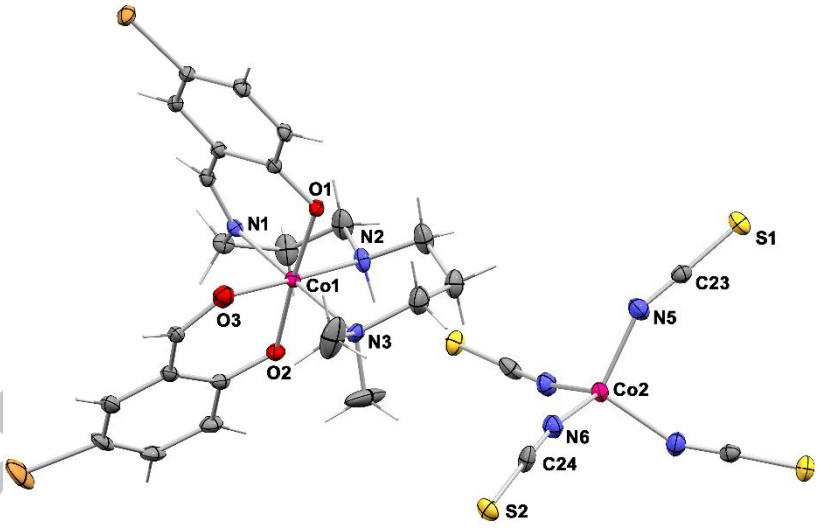

Fig. 3. A partial crystal structure of $[Co(L)(Br\text{-}sal)]_2[Co(NCS)_4]$ (**4**) with selected atom labelling scheme. One of the symmetry-related complex cations is omitted for clarity. Ellipsoids are drawn in 30% probability.

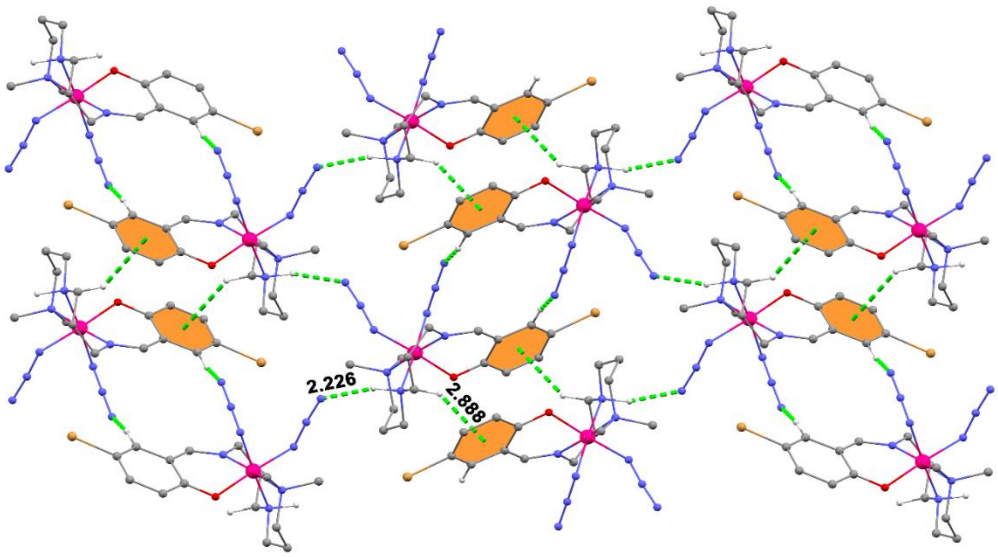

Fig. 4. A part of packing diagram showing hydrogen bonding and C–H···π interactions in **2**

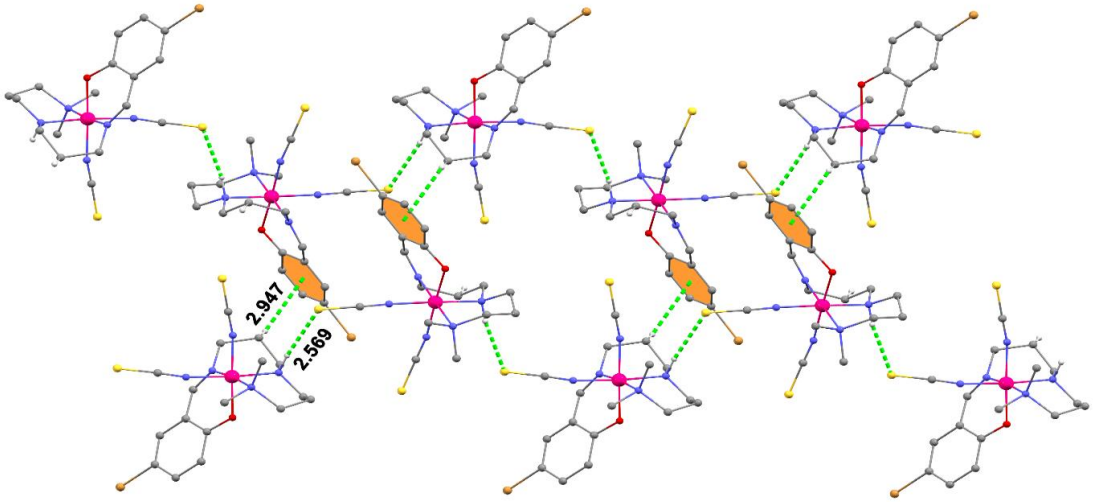

Fig. 5. A part of crystal packing of **3** displaying hydrogen bonding and C–H···π interactions.

Complex **4** crystalizes in the monoclinic C2/c space group in which the asymmetric unit includes a complete set of the complex cation of composition $[Co(L)(Br\text{-}sal)]^{+}$ on general position and a half of $Co(NCS)_4^{2-}$ unit on a two-fold axis. The geometry of $Co(NCS)_4^{2-}$ is a distorted tetrahedral in which thiocyanate ions coordinate cobalt(II) centre through the nitrogen atoms [56−60]. The oxidation state of cobalt in $Co(NCS)_4^{2-}$ is further ensured by the

room temperature magnetic study which results the magnetic moment value of 4.03 B.M, consisting with cobalt(II) center in tetrahedral geometry. The bond angles (N–Co–N) varying in the range 101.0(2)–112.1(2)º support the distorted tetrahedral structure of the complex anion. In complex cation $[Co(L)(Br\text{-}sal)]^+$, the geometry of cobalt(III) centre is best described as a distorted octahedral structure and it is coordinated by one deprotonated Schiff base ligand and a 5-bromosalicylaldehyde ion resulting from the hydrolysis of the Schiff base during complexation process. Like complexes **2** and **3**, the Schiff base ligand also coordinates the metal centre in the tetradentate fashion. The Co–N bond distances of imine, secondary and tertiary amines are 1.930(3), 2.005(3) and 2.091(3) Å, respectively, which are comparable to bond distances observed in **2** and **3** and also in the reported low-spin octahedral cobalt(III) complexes with similar coordination environments [53,56,57]. The Co–O (phenolate) and Co–O (Br-sal) bond distances are 1.888(3), 1.884(3) and 1.910(3), respectively, which are also comparable to the literature data. The Co–N bond distances associated with amine and imine nitrogen atoms are similar as that found in **2** and **3**. Different types of noncovalent interactions like hydrogen bonding and C–H···π interaction are responsible for the stability of the solid-state architecture of **4** (Fig. S6).

3.3 Electrochemical studies

The redox flexibility of the transition metal ion residing at the active site of metalloenzyme plays vital role in the biocatalytic oxidation of various biologically important organic compounds. Therefore, the electrochemical study of the enzymatic models could disclose their ability of functioning biomimetic catalysis. In this regard, the electrochemical properties of all complexes were examined in methanol in presence of 0.1 M tetrabutylammonium perchlorate as a supporting electrolyte. Cyclic voltammograms of **1** − **3** are displayed in Fig. 6, while Fig. 7 shows the electrochemical behaviour of **4**. Cyclic

voltammograms of **1**–**3** consist of an irreversible reduction response in the range –0.61 to –1.01 V, which is associated with the reduction of cobalt(III) to cobalt (II) at the electrode surface. The cyclic voltammogram of **4** also consists of a similar irreversible reductive response at –0.77 V. Additionally, an irreversible oxidative response was observed in **4** at 0.96 V. The reduction process is as usual responsible for the reduction of cobalt (III) to cobalt (II) of the complex cation at the electrode surface, while the oxidative response is due to the oxidation of cobalt (II) to cobalt (III) of the complex anion of formula $[Co(SCN)_4]^{2-}$.

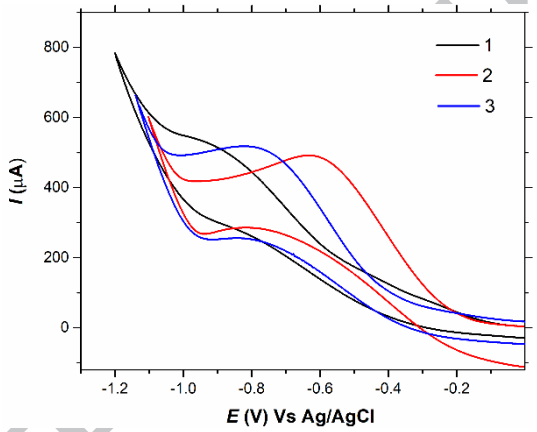

Fig. 6. Cyclic voltammograms of **1**–**3** in methanol at room temperature containing tetrabutylammonium perchlorate as a supporting electrolyte at a scan rate 100 mV s^{-1}.

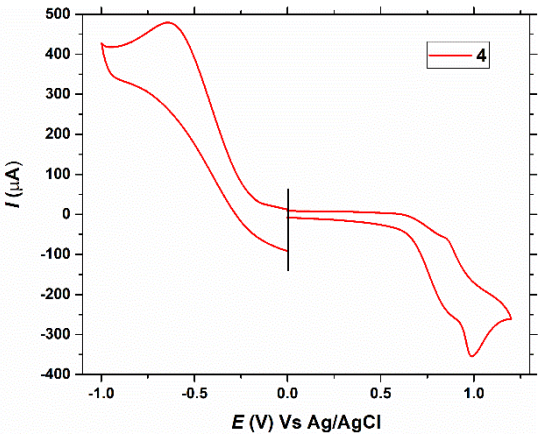

Fig. 7. Cyclic voltammogram of **4** in methanol at room temperature containing tetrabutylammonium perchlorate as a supporting electrolyte at a scan rate 100 mV s^{-1}.

3.4 Catalytic oxidation of o-aminophenols

UV-vis spectrophotometric method was applied to study oxidation of *o*-aminophenol (OAPH), by molecular dioxygen in presence of catalytic amount of the complexes in dioxygen-saturated methanol at room temperature [33]. In this context, 5.0 $\times 10^{-5}$ M methanolic solution of the complexes were allowed to react with a 1.0 $\times 10^{-2}$ M solution of OAPH. The progress of the reaction was monitored UV–vis spectrophotometrically at a regular time interval of 5 min, and the time-dependent spectral profiles for aerobic oxidation of OAPH catalysed by **2** and **3** are depicted in Fig. 8, while Fig. S7 represents the oxidation of OAPH by **1** and **4**. These spectral scans show the cumulative growth of spectral band at *ca*. 434 nm, which indicate the accumulation of 2-aminophenoxazinone as a function of time [61]. Careful inspection of these spectral scans at least qualitatively suggests that complex **2** and **3** are efficient catalysts for the oxidation of OAPH, while **1** and **4** are less reactive. Furthermore, a blank test was performed under same experimental condition in absence of the catalysts, where no such significant growth of spectral band is observed, supporting the role of catalysts in such reaction. In order to inculcate the catalytic efficiency of these complexes detailed kinetic study is performed in which 1.0×10^{-5} M solutions of the complexes were reacted with excess substrate at the pseudo-first-order condition and initial rates were evaluated. Plots of initial rate versus concentration of the substrate for oxidation of OAPH catalyzed by **1**−**4** show a typical rate saturation kinetics (Fig 9, Fig. S8), indicating the course of reaction proceeds through formation of a stable complex-substrate aggregate. These rate saturation profiles can be analyzed applying the Michaelis–Menten model to evaluate kinetic parameters V_{max}, K_M, and K_{cat} (Table 3). The turnover numbers (TON) of the catalysts were then calculated by dividing the value of V_{max} by the concentration of catalyst used and values are found to be 3.79, 51.74, 48.40 and 11.84 h^{-1} for **1**–**4**, respectively.

Literature data reveal that a fair number of model oxidations of *o*-aminophenol have been carried out to mimic phenoxazinone synthase activity to gain insight into the possible mechanism and to check efficiency of the synthetic analogues. In comparison to the literature data, it is clear that although **1** and **4** are less reactive but **2** and **3** are efficient catalysts for oxidation of *o*-aminophenol [45] The catalytic efficiency of the present compounds is slightly higher than the reported analogous compounds by us [50]. In previous cases, ethoxy or methoxy substitution at ortho position of the donor phenolate group of the Schiff base ligands may increase the steric crowding around the coordination sphere of the metal centre, leading to slightly weaker complex-substrate adduct formation ability, while in the present case no such effect may be expected as Br is substituted at para position with respect to the donor phenolate group. It is to be further noted that the catalytic oxidation of some substituted *o*-aminophenols and isolations and characterizations of their oxidised products were conducted with native enzyme and its models, but the detailed kinetic studies were not available in the literature. Therefore, it could be worthy to carry out the detailed kinetic investigations with some substituted *o*-aminophenols to get further insights into the reactive intermediates and the mechanistic details of the catalytic reactions and finally to establish the structure-reactivity correlation of the catalysts. Accordingly, the reaction kinetics of aerobic oxidation of 2-amino-5-methylphenol catalysed by the most reactive compounds **2** and **3,** leading to production of 2-amino-4,4a-dihydro-4a-7-dimethyl-3*H*-phenoxazineone (Phx-2), was carried out UV-vis spectrophotometrically (Fig. 10). Like *o*-aminophenol, the catalytic oxidation of this substituted *o*-aminophenol proceeds through the formation of a stable catalyst-substrate intermediate as suggested by the rate saturation kinetics (Fig 11) before the redox degradation of the intermediate in the rate determining step. Detailed kinetic analysis further gives us values of various kinetic parameters V_{max}, K_M, and K_{cat} which along with turnover numbers are given in Table 3.

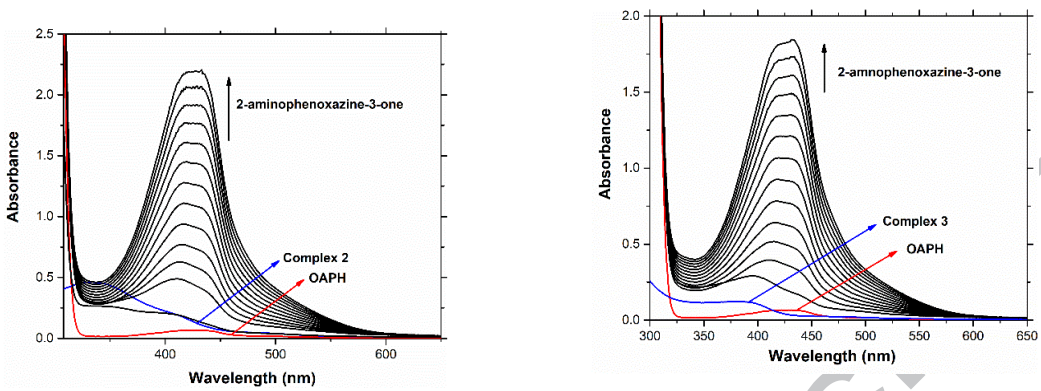

Fig. 8. UV-vis spectral profile for the aerobic oxidation of *o*-aminophenol (1.0×10^{-2} M) catalysed by **2** and **3** (5.0×10^{-5} M) in methanol. The spectra were recorded at 5 min intervals under aerobic conditions at room temperature

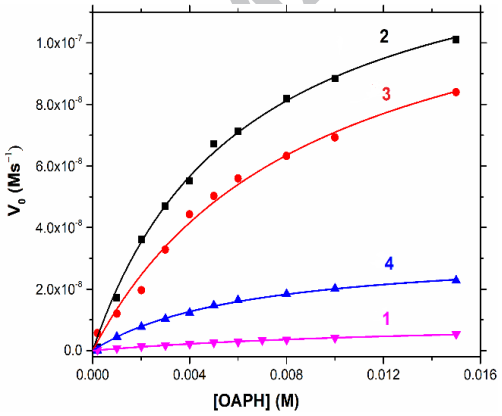

Fig. 9. Plots of initial rate versus substrate concentration for the aerobic oxidation of OAPH in methanol catalysed by **1**–**4** at room temperature. Symbols and solid lines represent the experimental and simulated profiles, respectively.

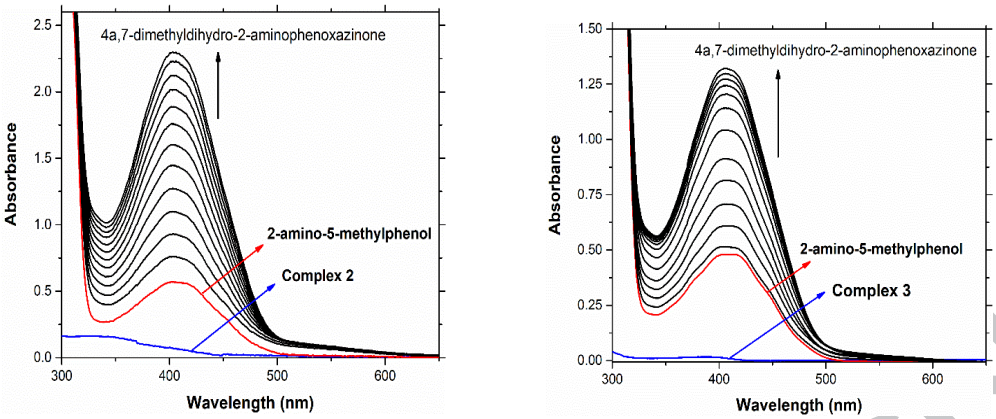

Fig. 10. Time dependent spectral scan showing growth of 4a,7-dimethyldihydro-2-aminophenoxazinone at 405 nm upon addition of 2-amino-5-methylphenol to a solution containing **2** or **3** in dioxygen-saturated methanol. The spectra were recorded at 5 min intervals under aerobic conditions at room temperature

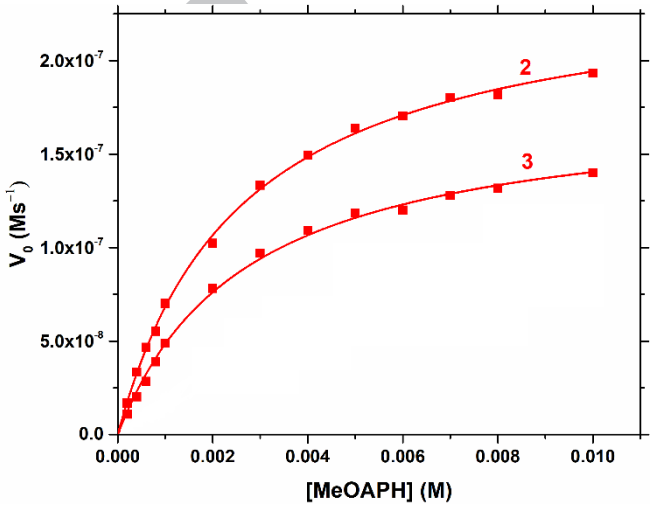

Fig. 11. Initial rate versus substrate concentration plot for the oxidation of 2-amino-5-methylphenol in dioxygen-saturated methanol catalysed by **2** or **3** at room temperature. Symbols and solid lines represent the experimental data and theoretical fit, respectively.

Table 3: Kinetic parameters of phenoxazinone synthase like activity for complexes **1**–**4**.

Substrate	Catalyst	V_{max} (Ms^{-1})	K_M (M)	k_{cat} (h^{-1})
OAPH	**1**	$(1.05 \pm 0.06) \times 10^{-8}$	$(1.52 \pm 0.15) \times 10^{-2}$	3.79
	2	$(1.44 \pm 0.04) \times 10^{-7}$	$(6.16 \pm 0.43) \times 10^{-3}$	51.74
	3	$(1.34 \pm 0.08) \times 10^{-7}$	$(8.95 \pm 1.1) \times 10^{-3}$	48.40
	4	$(3.29 \pm 0.10) \times 10^{-8}$	$(6.39 \pm 0.42) \times 10^{-3}$	11.84
2-amino-5-methylphenol	**2**	$(2.44 \pm 0.03) \times 10^{-7}$	$(2.59 \pm 0.86) \times 10^{-3}$	88.01
	3	$(1.78 \pm 0.03) \times 10^{-7}$	$(2.69 \pm 0.13) \times 10^{-3}$	64.14

3.5 Proposed mechanism, comparative catalysis and mass spectrometry

Among the several factors that can affect the catalytic efficiency of the synthetic analogues, the electronic environment around the metal centers and the labile position(s) at metal sites for substrate binding are the most crucial factors behind their efficient activities. In present systems, although the reduction potentials of the cobalt(III) centres are comparable, the excellent catalytic activity of **2** and **3** over **1** and **4** is mainly due to the ease of formation of stable complex-substrate intermediates by the replacement of labile sites (azide ions in **2** and thiocyanate ions in **3**) from the metal centres. Therefore, the course of catalytic reaction proceeds through the inner sphere electron transfer pathway in **2** and **3**, which is expected to be quite faster than the outer sphere electron transfer pathway that follows when **1** and **4** are used as catalysts where the metal centres are coordinatively saturated and no labile position is available for substrate binding. However, the better lability of azide over thiocyanate ion is responsible for somewhat greater reactivity of azide complex (**2**) compared to thiocyanate analogue (**3**). From the kinetic data, it is also clear that the catalytic oxidation of methyl substituted *o*-aminophenol is rather favourable than that of *o*-aminophenol itself which is quite reasonable as the electron donating methyl substitution facilitates the oxidation process.

But it ultimately produces dihydro-aminophenoxazinone chromophore instead of aminophenoxazinone chromophore as that methyl substitution blocks the final two-electrons oxidation step (scheme 3).

The mass spectral study could provide valuable information regarding the product and intermediate species that helps to establish the catalytic pathway of phenoxazinone synthase-like activity. Accordingly, the electrospray ionization mass spectra of a reactive compound **3** in presence of 20 equivalents of *o*-aminophenol or 2-amino-5-methylphenol in methanol were recorded and are displayed in Fig. 12 and 13, respectively. When *o*-aminophenol was used as a substrate, the basal peak was found at m/z = 110.12, which is nothing but the protonated species of substrate itself (calcd. m/z = 110.06), while for substrate 2-amino-5-methylphenol the basal peak at m/z = 243.23 is matched with the protonated species of the product 3-amino-1,4a-dihydro-4a-8-dimethyl-2*H*-phenoxazine-2-one (calcd. m/z = 243.11). Moreover, a product related peak at m/z = 213.17 (calcd. m/z = 213.06), consisting of the protonated species of the 2-aminophenoxazinone, is observed in the mass spectrum when *o*-aminophenol was used as a substrate. Similarly, a peak at m/z = 124.14 (calcd. m/z = 124.08) related to protonated species of substrate itself was found in the mass spectrum when 2-amino-5-methylphenol was used as a substrate. In both cases, a common peak at m/z = 741.45 (calcd. m/z = 741.19) is found in the mass spectra that indicates a species of composition $[(HL)_2+H_2O+K]^+$. The appearance of two other peaks at m/z 509.30 (calc. 509.10) for substrate *o*-aminophenol and m/z 521.32 (calc. 521.10) for substrate 2-amino-5-methylphenol are quite interesting as they support the formation of complex-substrate intermediate species of compositions $[(CoL)(OAPH)+H]^+$ and $[(CoL)(2\text{-amino-5-methylphenolate})]^+$, respectively. These observations clearly establish the ease of formation of stable complex-substrate aggregates, exploiting the stronger chelating ability of *o*-aminophenolate ions by the removal of terminal pseudohalide ions. The peak at m/z = 215.18 is also deserved to be

special mention as that is related to a monocationic species of an important reactive intermediate **II-B** (calcd. m/z = 215.08) produced during the course of oxidative coupling of *o*-aminophenol as drown in scheme 3.

We are now at the right position where both the mass spectral study and kinetic data clearly suggest that the catalytic cycle for the aerobic oxidation of *o*-aminophenol catalysed by **2** and **3** starts with the formation of a stable complex-substrate aggregate by the substitution of two coordinated pseudohalides by *o*-aminophenolate ion. This complex-substrate intermediate generates *o*-aminophenolate radical through the inner sphere electron transfer from *o*-amionophenolate to the cobalt(III) centre in the rate determining step. Being unstable the OAP radical thereafter is oxidised to *o*-benzoquinone monoamine (BQMI) in several ways including disproportionation of the OAP radical itself. The intermediate (BQMI) undergoes oxidative coupling with another molecule of OAP to produce a reactive intermedia **I-B**, followed by two electrons oxidation with molecular oxygen to produce another reactive intermediate **II-B** as supported by mass spectral study, which ultimately gives final product 2-aminophenoxazinone through the oxidative dehydrogenation of intermediate **II-B** as shown in Scheme 3. Similar mechanistic pathway is also applicable for catalytic oxidation of 2-amino-5-methylphenol in which methyl substitution does not inhibit the formation of a stable complex-substrate intermediate. Even that methyl substitution does not inhibit the coupling of two aminophenols, but the final 2-electrons oxidation was blocked by methyl substitution, leading to the formation of dihydro-phenoxazinone chromophore instead of phenoxazinone chromophore as found for the oxidation of *o*-aminophenol itself (see Scheme 3).

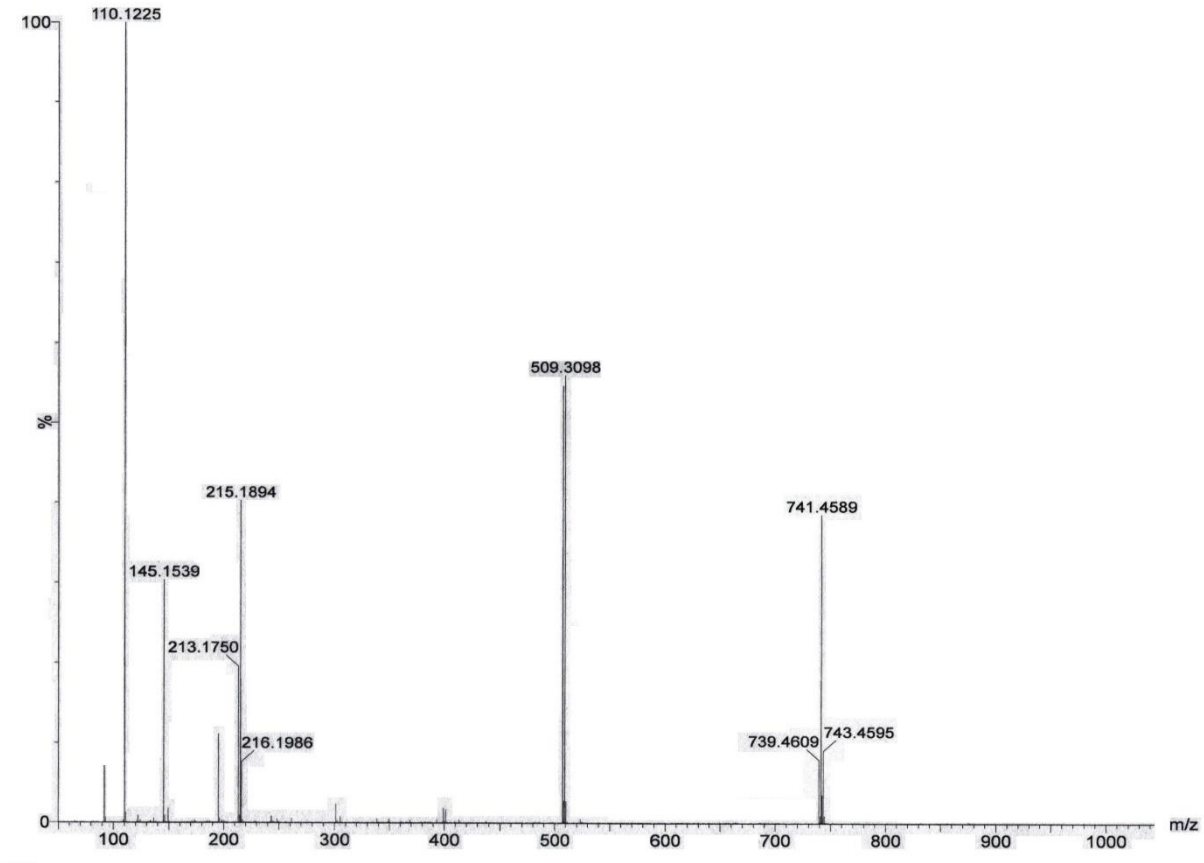

Fig. 12. Electrospray ionization mass spectrum (ESI-MS positive) of a 1:20 mixture of complex **3** and *o*-aminophenol in methanol recorded after 10 min of mixing.

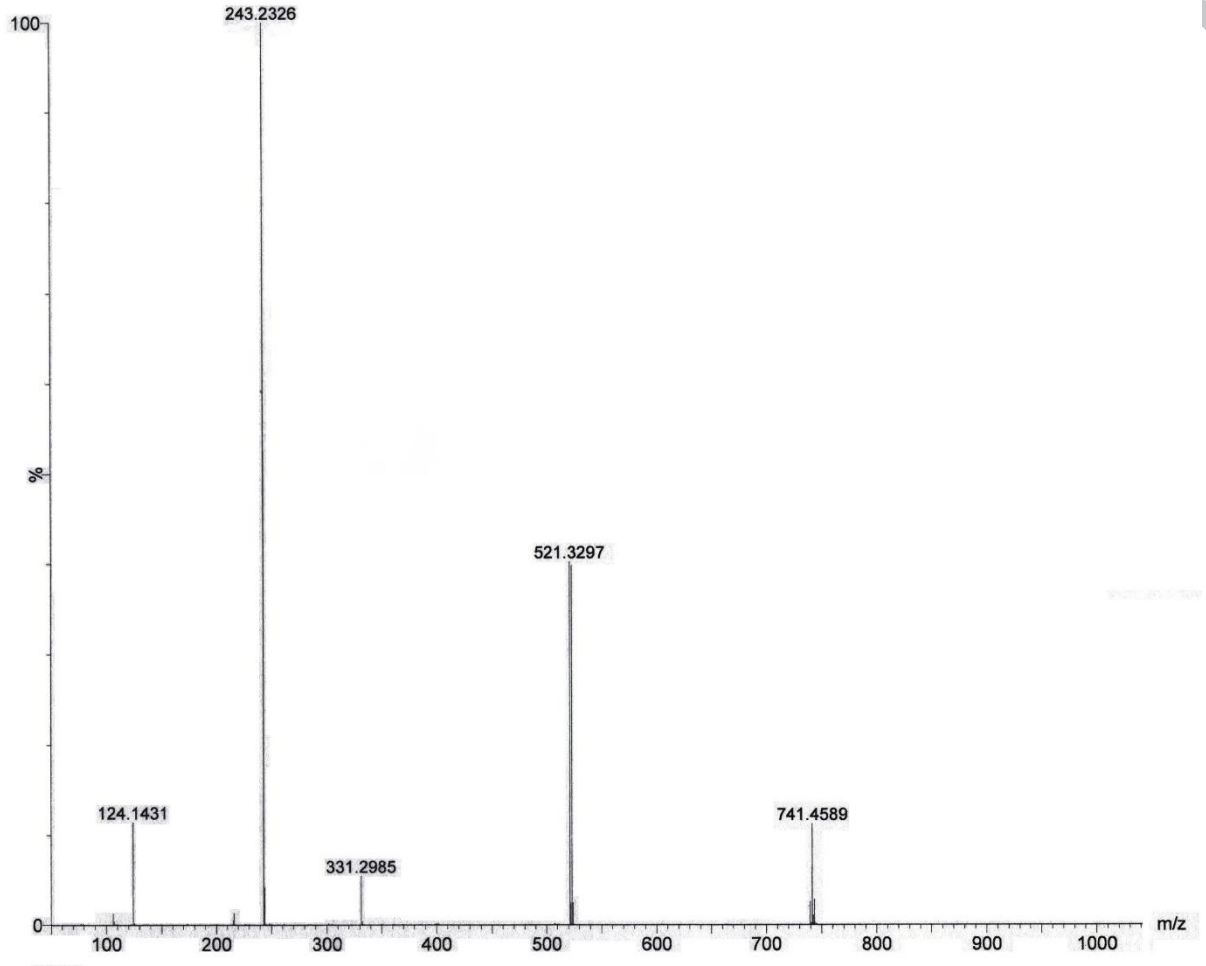

Fig. 13. Electrospray ionization mass spectrum (ESI-MS positive) of a 1:20 mixture of complex **3** and 2-amino-5-methylphenol in methanol recorded after 10 min of mixing.

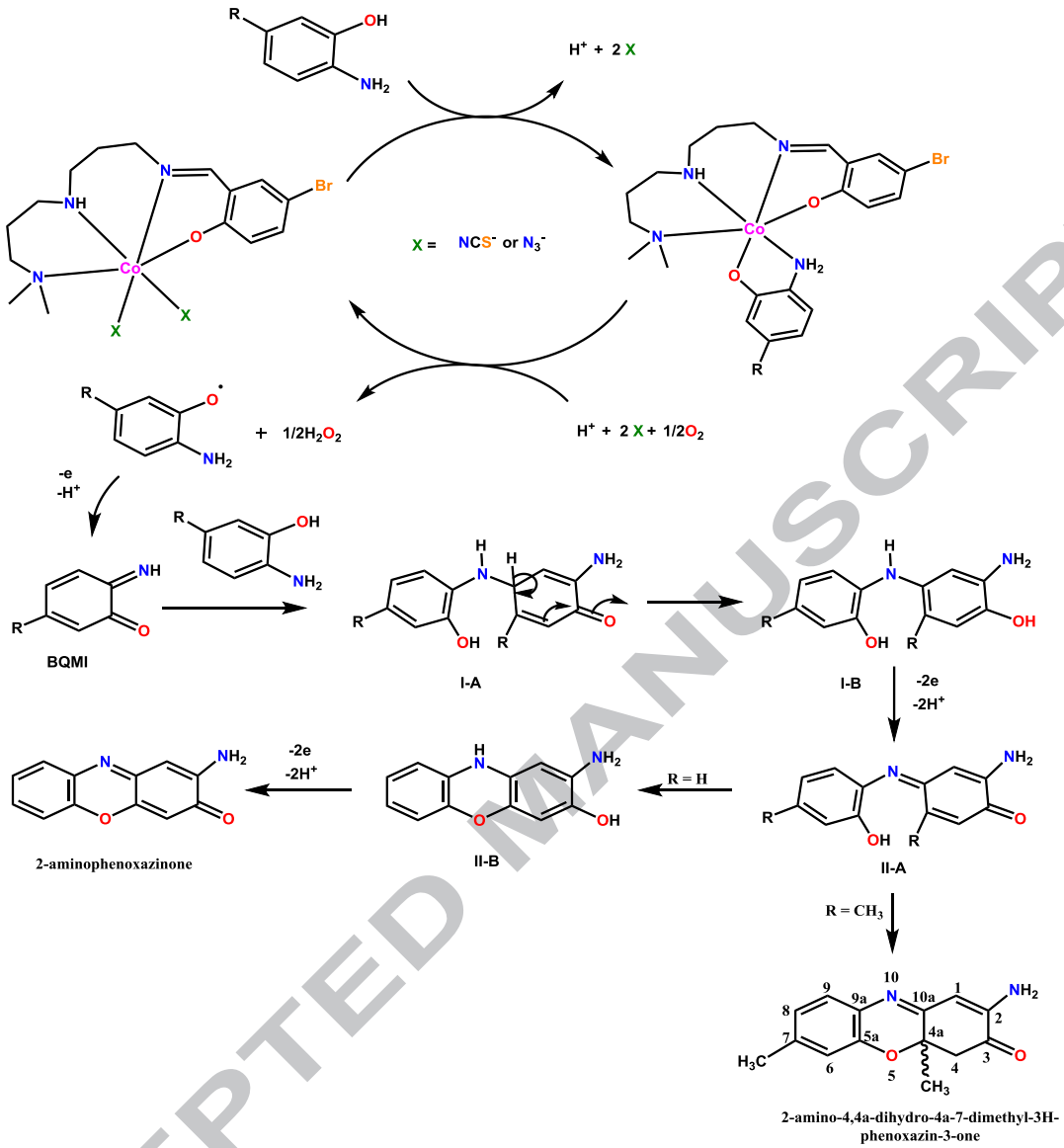

Scheme. 3. Proposed mechanistic pathway for the aerobic oxidation of *o*-aminophenols catalysed by **2** and **3**.

4. Conclusions

A new tetradentate N_3O donor Schiff base ligand has been synthesized by the condensation reaction of *N*,*N*-dimethyldipropylenetriamine and 5-bromosalicylaldehyde. This Schiff base ligand was allowed to react with cobalt(II) ions in presence of different counter ions that resulted diverse cobalt complexes where influence of both counter ions and the solvents on

structural diversity has been observed. All these complexes exhibit phenoxazinone synthase mimicking activity, but the reactivity of **2** and **3** is significantly higher than that of **1** and **4**. The available labile sites for the substrate binding in **2** and **3** is the main reason behind the stronger activity of **2** and **3** than the others. Literature reports reveal that although the catalytic oxidation of some substituted *o*-aminophenols and isolations and characterizations of their oxidised products were carried out with the native enzyme and its models, but the detailed kinetic studies were not available in the literature. Herein, we have examined the detailed kinetic studies of the aerobic oxidation of two substituted o-aminophenol, namely 2-amino-5-methylphenol, using **2** and **3** as catalysts. The present results disclose that the catalytic oxidation of methyl substituted *o*-aminophenols is much favourable than the oxidation of *o*-aminophenol itself which is due to the electron donating effect of methyl substitution, leading to the facile oxidation of these substrates. Interestingly, this methyl substitution does not inhibit the formation of a stable complex-substrate intermediate in the catalytic cycle and the oxidative coupling of two *o*-aminophenols as well, but the final two-electrons oxidation step was blocked by methyl substitution, leading to the formation of dihydro-phenoxazinone chromophore instead of phenoxazinone chromophore that observed for oxidation of *o*-aminophenol itself. ESI mass spectral study provides significant information from which the mechanistic pathway of functioning such catalytic activity has been explored.

Acknowledgements

A. P. also gratefully acknowledges the financial support of this work by the University Grant Commission, India (Sanction no. F. PSW-229/15-16(REO)). Panskura Banamali College acknowledges the grants received from Department of Science and Technology (DST), Govt.

of India through FIST program (SR-FIST-Col/295 dated 18/11/2015). The authors thank Jadavpur University, Kolkata for providing the Mass spectral facility.

Supplementary data

† Electronic supplementary information (ESI) available: The electronic supplementary information file contains Figs. S1–S8. CCDC 1874230-1874233 contain the supplementary crystallographic data for **1**–**4**, respectively. For ESI and crystallographic data in CIF or other electronic format see DOI: To be filled by the publisher.

References

[1] S. I. Murahashi, Y. Imada, in Transition Metals for Organic Synthesis, ed. M. Beller, C. Bolm, 2nd edn, Wiley-VCH, Weinheim, Germany. vol. 2 (2004) 497.

[2] J. Gómez, G. Garcia-Herbosa, J. V. Cuevas, A. Arnáiz, A. Carbayo, A. Muñoz, L. Falvello, P. E. Fanwick, Inorg. Chem. 45 (2006) 2483−2493.

[3] K.M. Gligorich, M.S. Sigman, Chem. Commun. (2009) 3854–3867.

[4] J. Piera, J.E. Backvall, Angew. Chem. Int. Ed. 47 (2008) 3506–3523.

[5] S.S. Stahl, Science 309 (2005) 1824–1826.

[6] T. Punniyamurthy, S. Velusamy, J. Iqbal, Chem. Rev. 105 (2005) 2329–2363.

[7] S.S. Stahl, Angew. Chem. Int. Ed. 43 (2004) 3400–3420.

[8] T. Funabiki (Ed.), Dioxygenases in Catalysis by Metal Complexes, Oxygenases and Model Systems, Kluwer Academic, Dordrecht (1997), 19.

[9] J.P. Klinman, J. Biol. Inorg. Chem. 16 (2011) 1.

[10] I. Bertini, H.B. Gray, S.J. Lippard, J.S. Valentine (Eds.), Dioxygen Reactions in Bioinorganic Chemistry, University Science Books, Sausalito (1994) 253.

[11] The chemistry and activation of dioxygen species (O_2, O_2^- and H_2O_2) in biology, in: A.E. Martell, D.T. Sawyer (Eds.), Oxygen Complexes and Oxygen Activation by Transition Metals, Plenum, New York (1988) 131.

[12] E. I. Solomon, T. C. Brunold, M. I. Davis, J. N. Kemsley, S. K. Lee, N. Lehnert, F. Neese, A. J. Skulan, Y. S. Yang, J. Zhou, Chem. Rev. 100 (2000) 235−350.

[13] (a) E. I. Solomon, R. Sarangi, J. S. Woertink, A. J. Augustine, J. Yoon, S. Ghosh, Acc. Chem. Res. 40 (2007) 581−591. (b) A. Guha, T. Chattopadhyay, N. D. Paul, M. Mukherjee, S. Goswami, T. K. Mondal, E. Zangrando, D. Das, Inorg. Chem. 51 16 (2012) 8750−8759.

[14] E. G. Kovaleva, J. D. Lipscomb, Nat. Chem. Biol. 4 (2008) 186−193.

[15] H. Arakawa, M. Aresta, J. N. Armor, M. A. Barteau, E. J. Beckman, A. T. Bell, J. E. Bercaw, C. Creutz, E. Dinjus, D. A. Dixon, K. Domen, D. L. DuBois, J. Eckert, E. Fujita, D. H. Gibson, W. A. Goddard, D. W. Goodman, J. Keller, G. J. Kubas, H. H. Kung, J. E. Lyons, L. E. Manzer, T. J. Marks, K. Morokuma, K. M. Nicholas, R. Periana, L. Que, J. Rostrup-Nielson, W. M. H. Sachtler, L. D. Schmidt, A. Sen, G. A. Somorjai, P. C. Stair, B. R. Stults, W. Tumas, Chem. Rev. 101 (2001) 953–996.

[16] T. Punniyamurthy, S. Velusamy, J. Iqbal, Chem. Rev. 105 (2005) 2329–2363.

[17] P. Chaudhuri, K. Wieghardt, Prog. Inorg. Chem. 50 (2001) 151–216.

[18] R. H. Holm, E. I. Solomon, Chem. Rev. 104 (2004) 347–1200.

[19] C. Mukherjee, T. Weyhermüller, E. Bothe, E. Rentschler, P. Chaudhuri, Inorg. Chem. 46 (2007) 9895–9905.

[20] P. Chaudhuri, K. Wieghardt, T. Weyhermüller, T. K. Paine, S. Mukherjee, C. Mukherjee, Biol. Chem. 386 (2005) 1023–1033.

[21] U. Jhan, Top. Curr. Chem. 320 (2004) 323−452.

[22] S. E. Allen, R. R. Walvoord, R. Padilla-Salinas, M. C. Kozlowski, Chem. Rev. 113 (2013) 6234−6458.

[23] T. K. Paine, L. Que, Jr, Struct. Bond. 160 (2014) 39−56.

[24] S.S. Stahl, Science 309 (2005) 1824−1826.

[25] L.I. Simándi (Ed.), Advances in Catalytic Activation of Dioxygen by Metal Complexes, Springer, New York, (2003).

[26] B. Meunier (Ed.), Biomimetic Oxidations Catalyzed by Transition Metal Complexes, Imperial College, London, (2000).

[27] M. Shyamal, T. K. Mandal, A. Panja, A Saha. RSC Adv. 4 (96) (2014) 53520-53530.

[28] N. C. Jana, P. Brandão, A. Panja. J. Inorg. Biochem 159 (2016) 96–106.

[29] A. Panja, N.C. Jana, A. Bauzá, S. Adak, T.M. Mwania, D.M. Eichhorn, A. Frontera, Chemistry Select. 2(6) (2017) 2094-2105.

[30] A. Panja, P. Guionneau, Dalton Trans. 42 (2013) 5068−5075.

[31] A. Panja, RSC Adv. 4 (2014) 37085–37094.

[32] T. Horvath, J. Kaizer, G. Speier, J. Mol. Catal. A: Chem. 215 (2004) 9–15.

[33] L. I. Simandi, M. Tatiana, Z. May, G. Besenyei, Coord. Chem. Rev. 245 (2003) 85–93.

[34] T. M. Simandi, L. I. Simandi, M. Gyor, A. Rockenbauer, A. Gomory, Dalton Trans. (2004) 1056–1060.

[35] C. E. Barry, P. G. Nayar, T. P. Begley, J. Am. Chem. Soc. 110 (1988) 3333–3342.

[36] E. Frei, Cancer Chemo ther. Rep. Part 1.58 (1974) 49–54.

[37] U. Hollstein, Chem. Rev. 74 (1974) 625–652.

[38] E. Katz, H. Weissbach, J. Biol. Chem. 237 (1962) 882–886.

[39] S. Shimizu, M. Suzuki, A. Tomoda, S. Arai, H. Taguchi, T. Hanawa, S. Kamiya, J. Tohoku, Exp. Med. 203 (2004) 47–52.

[40] L.I. Simándi, T.M. Simándi, Z. May, G. Besenyei, Coordination chemistry reviews. 245(1) (2003) 85−93.

[41] M. Hassanein, M. Abdo, S. Gerges, S. El-Khalafy, Journal of Molecular Catalysis A: Chemical. 287(1) (2008) 53−56.

[42] T.M. Simándi, L.I. Simándi, M. Győr, A. Rockenbauer, Á. Gömöry, Dalton Transactions. 7 (2004) 1056−1060.

[43] A. C. Sousa, M. C. Oliveira, L. O. Martins, M. P. Robalo, Green Chem. 16 (2014) 4127−4136.

[44] J. Kaizer, G. Baráth, R. Csonka, G. Speier, L. Korecz, A. Rockenbauer, L. Párkányi, Journal of inorganic biochemistry. 102(4) (2008) 773−780.

[45] S.K. Dey, A. Mukherjee, Coord. Chem. Rev. 310 (2016) 80−115.

[46] S. Sagar, S. Sengupta, A. J. Mota, S. K. Chattopadhyay, A. E. Ferao, E. Riviere, W. Lewis, S. Naskar, Dalton Trans. 46 (2017) 1249–1259.

[47] A. Jana, N. Aliaga-Alcalde, E. Ruiz, S. Mohanta, Inorg. Chem. 52 (2013) 7732–7746.

[48] P. Mahapatra, S. Ghosh, S. Giri, V. Rane, R. Kadam, M. G. B. Drew, A. Ghosh, Inorg. Chem. 56 (9) (2017**)** 5105–5121.

[49] A. Company, L. Gomez, R. Mas-Balleste, I. V. Korendovych, X. Ribas, A. Poater, T. Parella, X. Fontrodona, J. Benet- Buchholz, M. Sola, L. Que Jr, E. V. Rybak-Akimova, M. Costas, Inorg. Chem. 46 (2007) 4997–5012.

[50] (a) A. Panja, N.C. Jana, S. Adak, P. Brandão, L. Dlháň, J. Titiš, R. Boča, New J. Chem 41 (2017) 3143–3153. (b) A. Panja, N.C. Jana, P. Brandão, Molecular Catalysis, 449 (2018) 49–61. (c) A. Panja, N.C. Jana, P. Brandão, New Journal of Chemistry, 41(18) (2017) 9784–9795.

[51] G. M. Sheldrick, SADABS, University of Go¨ttingen, Germany, 1996.

[52] G. M. Sheldrick, Acta Crystallogr., Sect. A: Found. Crystallogr. 64 (2008) 112–122.

[53] A Panja, Dalton Trans. 43 (2014) 7760–7770

[54] S. Banerjee, P. Brandão, A. Bauzá, A. Frontera, M. Barceló- Oliverc, A. Panja, A. Saha, New J. Chem. 41 (2017) 11607–11618.

[55] A. Hazari, L. K. Das, A. Bauzá; A. Frontera A. Ghosh, Dalton Trans. 45 (2016) 5730−5740.

[56] A. Panja, M. Shyamal, A. Saha, T.K. Mandal, Dalton Trans. 43 (2014) 5443−5452.

[57] L. Mandal, S. Mohanta, Dalton Trans. 43 (2014) 15737−15751

[58] H. Mori, N. Sakurai, S. Tanaka, H. Moriyama, T. Mori, H. Kobayashi, A. Kobayashi Chem.Mater. 12 **(**2000) 2984−2987.

[59] S. Sen, P. Talukder, S. K. Dey, S, Mitra, G. Rosair, D. L. Hughes, G. P. A. Yap, G. Pilet, V. Gramlich, T. Matsushita, Dalton Trans. (2006) 1758.

[60] A. Ray, G. M. Rosair, R. Kadam S. Mitra, Polyhedron 28 (2009) 796−806.

[61] N. Sarkar, K. Harms, A. Bauzá, A. Frontera, S. Chattopadhyay, Chemistry Select. 2 (2017) 2975−2984. (b) K. Ghosh, K. Harms, S. Chattopadhyay, Polyhedron. 112 (2016) 6−17. (c) A. Panja, N. C. Jana, M. Patra, P. Brandão, C. E. Moore, D. M. Eichhorn, A. Frontera, J. Mol. Cat A. 412 **(**2016) 56–66.

Graphical Abstract (pictogram)

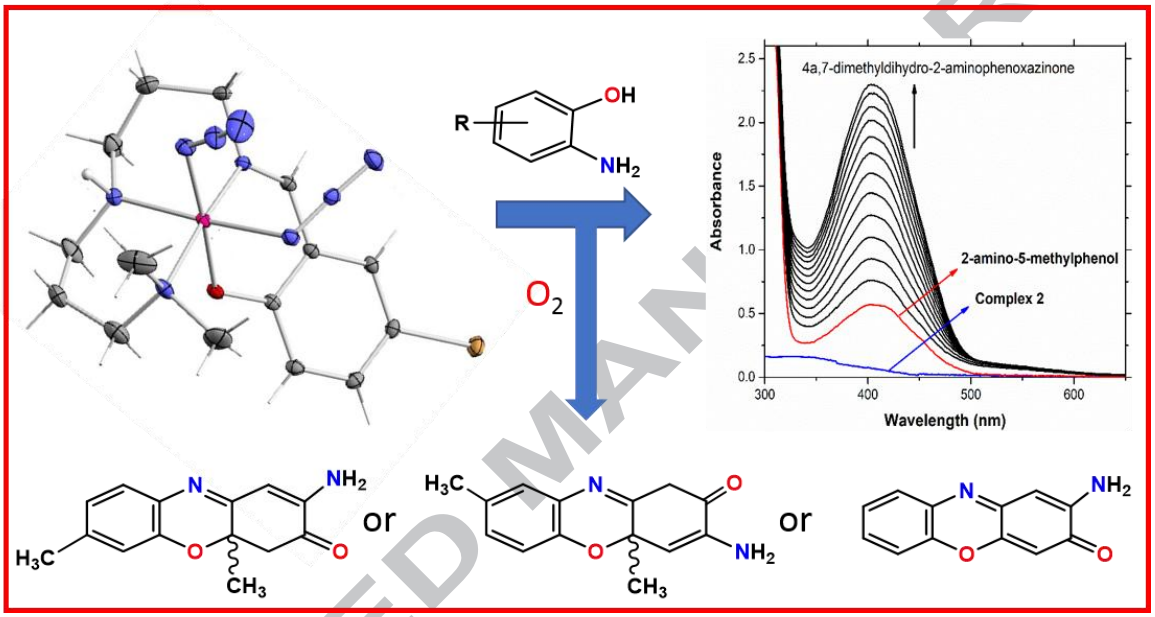

Graphical Abstract (synopsis)

Synthesis, structure and diverse coordination chemistry of cobalt(III) complexes derived from a Schiff base ligand and their biomimetic catalytic oxidation of *o*-aminophenols

Narayan Ch. Jana, Moumita Patra, Paula Brandão and Anangamohan Panja

Four new cobalt complexes with diverse structures exhibit catalytic oxidation of *o*-aminophenols, and their reactivity and the mechanistic pathway have been explored.